

Search for doubly charged scalars in type-II seesaw mechanism through photon fusion at the LHC^{*}

Hang Zhou (周航)^{1†}  Ning Liu (刘宁)^{2,3‡}

¹School of Microelectronics and Control Engineering, Changzhou University Changzhou 213164, China

²Physics Department and Institute of Theoretical Physics, Nanjing Normal University Nanjing 210023, China

³Nanjing Key Laboratory of Particle Physics and Astrophysics Nanjing 210023, China

Abstract: Small neutrino masses can be generated through the well-known seesaw mechanisms, among which the type-II scenario predicts a triplet scalar with doubly charged components. Except for the Drell-Yan production at the Large Hadron Collider (LHC), the doubly charged scalars $\Delta^{\pm\pm}$ can also be produced through photon fusion along with the ultraperipheral collision of protons, from which the outgoing protons can be detected by forward detectors at the LHC, providing a promising means to explore related new physics. We study the pair production through such processes at the 14 TeV LHC, focusing on the final states of $\mu^+\mu^+\mu^-\mu^-$ and $e^+e^+e^-e^-$ under the normal hierarchy (NH) and inverted hierarchy (IH) of the neutrino mass spectra, respectively. Promising sensitivity can be reached via our proposed search strategy. At a luminosity of 36.1 fb^{-1} (100 fb^{-1}), $m_\Delta \sim 430$ (520) GeV can be excluded at 95% C.L. under the NH via $\mu^+\mu^+\mu^-\mu^-$ state searching, while the mass bound can be extended to 730 (880) GeV under the IH via $e^+e^+e^-e^-$ states. The exclusion limits on m_Δ can be improved up to 1 TeV and even higher with integrated luminosity accumulated to 3 ab^{-1} .

Keywords: neutrino mass model, LHC phenomenology, search for BSM

DOI: 10.1088/1674-1137/ae2f52 **CSTR:** 32044.14.ChinesePhysicsC.50043103

I. INTRODUCTION

Neutrino oscillation experiments strongly motivate small yet non-zero neutrino masses, providing clear evidence for new physics beyond the Standard Model (SM) of particle physics. One of the most well-known and widely-studied schemes for this problem is the Weinberg dimension-5 operator $\mathcal{L} \propto \ell_L H H \ell_L / \Lambda$ [1], where ℓ_L and H refer to the $SU(2)_L$ doublet lepton and SM Higgs doublet, respectively. With a relatively high-scale cutoff Λ , tiny neutrino masses of Majorana nature can then be generated naturally after the electroweak symmetry breaking (EWSB). Ultraviolet completion of the Weinberg operator at tree level exists in only three ways, generally known as the three types of seesaw mechanisms [2–11], introducing to the SM right-handed neutrinos (type-I), $SU(2)_L$ triplet scalars (type-II) or $SU(2)_L$ triplet fermions (type-III). Different from type-I/III seesaws, which mix Dirac and Majorana-type masses, the type-II scenario generates neutrino masses via Yukawa couplings of the triplet scalar

Δ with the SM lepton doublets $m_\nu \sim Y_\nu v_\Delta$, where Y_ν is the neutrino Yukawa coupling and v_Δ the vacuum expectation value (VEV) of the neutral component of Δ . A seesaw style thus appears after the EWSB considering the mixing between the SM Higgs and triplet $v_\Delta \sim \mu v_0^2 / m_\Delta^2$, with the triplet mass m_Δ being orders larger than the electroweak scale $v_0 \sim 246$ GeV. The dimensional mixing parameter μ in the type-II seesaw is allowed to be naturally small enough according to the 't Hooft naturalness argument [12, 13] so that in such a scenario, the Yukawa coupling Y_ν not only relates neutrino oscillation experimental data to collider searches through dileptonic decay of the new scalar, but its mass m_Δ can also be low enough to be accessible at current collider experiments, including the Large Hadron Collider (LHC).

Searches for the triplet scalar at colliders and studies on the relevant features have been extensively conducted [14–20], as its charged components, especially the doubly charged ones, are predicted not only in the type-II seesaw but also in a variety of other beyond SM models,

Received 13 October 2025; Accepted 19 December 2025; Accepted manuscript online 20 December 2025

^{*} Supported by the National Natural Science Foundation of China (12405118) and the Natural Science Foundation of Jiangsu Province (BK20230623)

[†] E-mail: zhouhang@cczu.edu.cn

[‡] E-mail: liuning@njnu.edu.cn



Content from this work may be used under the terms of the Creative Commons Attribution 3.0 licence. Any further distribution of this work must maintain attribution to the author(s) and the title of the work, journal citation and DOI. Article funded by SCOAP³ and published under licence by Chinese Physical Society and the Institute of High Energy Physics of the Chinese Academy of Sciences and the Institute of Modern Physics of the Chinese Academy of Sciences and IOP Publishing Ltd

such as the left-right symmetric models [21–23], Zee-Babu model [24, 25], and Georgi-Machacek model [26, 27]. The most commonly considered production channels at hadron colliders are the Drell-Yan processes, where the doubly charged scalars are produced in pairs or in association with a singly charged one through a neutral or charged current, respectively. As these exotic scalars couple to the electroweak bosons via gauge interaction, their production cross sections through Drell-Yan processes can be predicted as a function of their masses. As an example, for $m_{\Delta^{++}} \sim 1$ TeV, the pair production cross section can reach ~ 0.1 fb at the leading order (LO) with acolliding energy of 14 TeV, and the next-to-leading order (NLO) QCD corrections can give a k -factor $k = \sigma^{\text{NLO}}/\sigma^{\text{LO}}$ in the range of $1.1 \sim 1.3$ [28, 29].

Regarding the decays, there are three modes of doubly charged scalars: dileptonic, dibosonic, and cascade decay channels, among which the dileptonic and dibosonic ones are the most studied for collider searches. It is the value of v_Δ that largely determines the dominance of these two modes. Assuming v_Δ far less than 10^{-4} GeV, the dileptonic decay channels $\Delta^{\pm\pm} \rightarrow \ell^\pm \ell'^\pm$ dominate. With this assumption of dileptonic dominance and equal branching ratios into different possible final states, that is, $\text{Br}(\Delta^{\pm\pm} \rightarrow \ell^\pm \ell'^\pm) = 1/6$ ($\ell, \ell' = e, \mu, \tau$), the ATLAS collaboration derived a stringent lower limit for the doubly charged scalar mass at 95% C.L. $m_\Delta > 1080$ GeV at the 13 TeV LHC using an integrated luminosity of 139 fb^{-1} [30]. With a larger $v_\Delta > 10^{-4}$ GeV, the dileptonic decay channels are highly suppressed due to the increasing v_Δ , and only diboson channels $\Delta^{\pm\pm} \rightarrow W^\pm W^\pm$ are relevant; the ATLAS collaboration obtained relatively weaker bounds at 200–220 GeV for a degenerate spectrum at the 13 TeV LHC with 36 fb^{-1} collected events [31]. In the parametric region of a moderate mass separation of $\Delta m \gtrsim 5$ GeV or even larger splitting, the third channel cascade decay $\Delta^{\pm\pm} \rightarrow \Delta^\pm W^{\pm*} \rightarrow \Delta^0 W^{\pm*} W^{\pm*}$ becomes dominant over the dileptonic and dibosonic ones if v_Δ is relatively close to 10^{-4} GeV by orders (either larger or smaller) [32]. For a non-degenerate spectrum with a mass difference of up to 100 GeV, lower limits of 350 and 230 GeV are obtained for pair and associated production, respectively, at $\sqrt{s} = 13$ TeV with a luminosity of 139 fb^{-1} [33]. Although most previous experimental searches have assumed degeneracy or a tiny mass splitting, it is allowed to be as large as $\Delta m \sim 40$ GeV for hundreds-of-GeV triplet Higgs bosons if considering the electroweak precision data, since heavy scalars' contribution to the oblique parameter T is compensated by the mass difference among the triplet components [32, 34]. Hence, the experimental bounds for doubly charged Higgs bosons are generally sensitive to different parametric regions of the model, mainly concerned with the triplet scalar VEV v_Δ and mass spectrum of the charged and neutral components. Due to the large hadronic background at the LHC, a

tiny v_Δ is typically assumed for a dominant dileptonic mode in experimental searches as well as phenomenological studies.

While the above-mentioned conclusions on experimental bounds are mostly drawn by taking the Drell-Yan production of triplet scalars into consideration, initial photon fusion from elastic collisions of protons, although receiving less attention, has become increasingly attractive recently as the forward detectors have been launched at the LHC, including the CMS-TOTEM Precision Proton Spectrometer (CT-PPS) [35] and ATLAS Forward Proton detector (AFP) [36]. These forward physics facilities (FPF) are located close to the colliding beams and around 220 meters from the collision point. With the FPFs installed successfully, new windows are opened to the elastic events at the LHC because the forward detectors are designed mainly to identify unsuccessfully colliding protons. Those protons go through what are generally known as ultraperipheral collisions (UPCs) and remain intact when reaching the forward detectors. Along with the UPC processes, initial photon fusion can occur because the electromagnetic field around the fast-moving protons can be approximated to on-shell photons (equivalent photon approximation; EPA). Accompanying the elastic collisions between protons, photon fusion can lead to pair production of charged particles, such as doubly charged scalars. Although it has been shown that the contribution from photon-fusion is less than that of neutral current Drell-Yan production [37, 38], the elastic nature of collisions will leave unique signatures of two unharmed protons reaching the forward detectors, forming a special topology with rapidity gaps between those forward protons and the central particles. These features make the photon fusion in UPC processes a new, promising way to search for new physics in the forward regions, which was not even possible before the launch of forward facilities. Utilizing forward proton-tagging, an increasing number of phenomenological studies have been conducted for probing new particles beyond the SM at the LHC, including supersymmetric dark matter candidates [39, 40], quasistable or nearly-degenerate charginos in specific SUSY scenarios [41–43], and multiple charged scalars in seesaw and left-right symmetric models [44–46].

In this paper, we propose a search strategy for probing degenerate doubly-charged scalars in the type-II seesaw model via tagging forward protons at the LHC, within the contexts of both normal and inverted hierarchies of neutrino mass spectra. In the next section, we concisely introduce the multiple scalars of the type-II seesaw and their production and decay at the hadron collider, as well as the connection to neutrino physics. Section III details the signals and presents the simulation. Section IV presents our proposed search strategies and results. Finally, we draw conclusions in Section V.

II. DOUBLY CHARGED SCALARS IN TYPE-II SEESAW MODEL

The seesaw mechanism of type-II for neutrino mass generation can be realized in a simple way by extending the SM with a complex scalar triplet lying in the adjoint representation of the weak group $SU(2)_L$,

$$\Delta = \begin{pmatrix} \frac{\Delta^+}{\sqrt{2}} & \Delta^{++} \\ \Delta^0 & -\frac{\Delta^+}{\sqrt{2}} \end{pmatrix}, \quad (1)$$

with hypercharge $Y_\Delta = 1$ as in the convention for the formula $Q = T_3 + Y$. A gauge-invariant and the most general renormalizable Lagrangian for the type-II seesaw scalar sector can be expressed as [47, 48]

$$\mathcal{L} \subset (D_\mu H)^\dagger (D^\mu H) + \text{Tr}[(D_\mu \Delta)^\dagger (D^\mu \Delta)] - V(H, \Delta), \quad (2)$$

where H is the SM Higgs doublet $H = (\phi^+, \phi^0)^T$ and $V(H, \Delta)$ represents the scalar potential, including contributions from the SM Higgs and triplet scalar [47, 48]

$$\begin{aligned} V(H, \Delta) = & -m_H^2 H^\dagger H + m_\Delta^2 \text{Tr}[\Delta^\dagger \Delta] + [\mu H^T i\sigma_2 \Delta^\dagger H + \text{h.c.}] \\ & + \frac{\lambda}{4} (H^\dagger H)^2 + \lambda_1 (H^\dagger H) \text{Tr}[\Delta^\dagger \Delta] + \lambda_2 [\text{Tr}(\Delta^\dagger \Delta)]^2 \\ & + \lambda_3 \text{Tr}[(\Delta^\dagger \Delta)^2] + \lambda_4 H^\dagger \Delta^\dagger \Delta H, \end{aligned} \quad (3)$$

where $m_{H,\Delta}^2$ are mass parameters for the SM Higgs and triplet scalar. λ and λ_{1-4} are quartic couplings that can be taken as real numbers without loss of generality. μ is the coupling for trilinear terms, which may violate lepton number conservation.

Besides the kinetic terms and scalar potential, the type-II seesaw introduces an additional Yukawa interaction between the triplet scalar and SM lepton doublets $L = (\nu_\ell, \ell)^T$ for neutrino mass generation:

$$\mathcal{L}_{Y_\Delta} = -y_\Delta L^T C i\sigma_2 \Delta L + \text{h.c.}, \quad (4)$$

where y_Δ is the Yukawa coupling and C the charge conjugation operator. Once the doublet and triplet scalars develop non-vanishing vacuum expectation values after the spontaneous electroweak symmetry breaking as v_0 and v_Δ , respectively, the seesaw mechanism works to generate Majorana masses of neutrinos

$$\mathcal{M}_\nu = \sqrt{2} Y_\Delta v_\Delta, \quad (5)$$

where the complex symmetric matrix \mathcal{M}_ν can be diagonalized using the PMNS mixing matrix U as $\mathcal{M}_\nu = U^* m_\nu U^\dagger$. The parameterization of the PMNS matrix can generally be expressed as follows [49]:

$$U = \begin{pmatrix} c_{12}c_{13} & s_{12}c_{13} & s_{13}e^{-i\delta} \\ -s_{12}c_{23} - c_{12}s_{13}s_{23}e^{i\delta} & c_{12}c_{23} - s_{12}s_{13}s_{23}e^{i\delta} & c_{13}s_{23} \\ s_{12}s_{23} - c_{12}s_{13}c_{23}e^{i\delta} & -c_{12}s_{23} - s_{12}s_{13}c_{23}e^{i\delta} & c_{13}c_{23} \end{pmatrix} \times \text{diag}\{e^{i\eta_1}, e^{i\eta_2}, 1\}, \quad (6)$$

where $c_{ij} = \cos\theta_{ij}$ and $s_{ij} = \sin\theta_{ij}$ with θ_{ij} being the mixing angles lying in the range of $[0, \pi/2]$ without loss of generality. δ and $\eta_{1,2}$ refer to Dirac and Majorana phases, respectively. Diagonal m_ν incorporates three physical neutrino masses mixed by three flavors through the mixing matrix, the entries of which can be largely determined by various neutrino oscillation experiments except for the minimal neutrino mass $\nu_{1/3}$, corresponding to normal hierarchy (NH)/inverted hierarchy (IH), and two Majorana phases. As the minimalization of the scalar potential in Eq. (3) leads to $v_\Delta \approx \mu v_0^2 / m_\Delta^2$ with the electroweak vacuum $v^2 = v_0^2 + v_\Delta^2 \approx 246^2 \text{ GeV}^2$, one can infer that either a large m_Δ or small μ can induce a small v_Δ , giving tiny neutrino masses in a seesaw manner. Besides, triplet scalar VEV contributes to radiative corrections for the ρ parameter in electroweak precision observables as a result of

modifications to W and Z masses, leading to the prediction $\rho \approx 1 - 2v_\Delta^2/v^2$. Given the current results for global fit $\rho = 1.00031 \pm 0.00019$ [49], an upper limit for v_Δ can be obtained around 2.8 GeV at 3σ C.L., far less than the doublet VEV v_0 . Because the non-diagonal Yukawa matrix y_Δ gives rise to lepton flavor violating processes, including $\mu^- \rightarrow e^+ e^- e^-$ and $\mu^- \rightarrow e^- \gamma$, upper bounds for the branching ratios of these rare decays [50, 51] can then be translated into a bound from below for v_Δ depending on $m_{\Delta^{**}}$:

$$v_\Delta \gtrsim 10^{-9} \text{ GeV} \times \frac{1 \text{ TeV}}{m_{\Delta^{**}}}, \quad (7)$$

exhibiting the order of magnitude of v_Δ for TeV-scale Δ^{**} [52, 53].

As stated briefly above in Section I, decay modes of the doubly charged scalars depend on the triplet VEV v_Δ and their mass spectrum. Decay width for the leptonic decay modes can be given as [32, 47, 48, 54]:

$$\Gamma(\Delta^{\pm\pm} \rightarrow \ell_i^\pm \ell_j^\pm) = \frac{m_{\Delta^{\pm\pm}}}{8\pi(1+\delta_{ij})} \left| \frac{\mathcal{M}_\nu^{ij}}{v_\Delta} \right|^2, \quad (8)$$

which, if $v_\Delta < 10^{-4}$ GeV, dominate over the gauge bosonic ones:

$$\Gamma(\Delta^{\pm\pm} \rightarrow W^\pm W^\pm) = \frac{g^4 v_\Delta^2}{8\pi m_{\Delta^{\pm\pm}}} \sqrt{1 - \left(\frac{2m_W}{m_{\Delta^{\pm\pm}}}\right)^2} \times \left[\left(\frac{m_{\Delta^{\pm\pm}}^2}{2m_W^2} - 1\right)^2 + 2 \right], \quad (9)$$

where i, j represent lepton flavors, δ_{ij} the Kronecker delta symbol, and g the weak gauge coupling. Cascade decay channels $\Delta^{\pm\pm} \rightarrow \Delta^\pm W^\pm$ are kinematically possible only if the mass difference $\Delta m = m_{\Delta^{\pm\pm}} - m_{\Delta^\pm} > 0$ and are dominant for a sufficiently large Δm of a few or tens of GeV [48], which is beyond the scope of the present work focusing on the case of a degenerate mass spectrum. For the case of non-degeneracy, relevant studies [48] and references therein can be referred to, where cascade decays are considered. In the present paper, considering the constraints from electroweak precision measurements and lepton flavor violating decays discussed above in Section I, we can safely assume a triplet VEV much smaller than 10^{-4} GeV so that only leptonic decay modes will be relevant in our following analysis of the collider search for the doubly charged Higgs bosons.

III. SIGNAL AND BACKGROUND

Different from the well-studied Drell-Yan production for the doubly charged scalars introduced in Section I, the present paper considers a search strategy through photon fusion pair production $\gamma\gamma \rightarrow \Delta^{\pm\pm} \Delta^{\mp\mp}$, where the initial photons come from equivalent photon approximation (EPA) alongside the UPCs of protons at the LHC. Two colliding protons remain intact in the final states to be tagged by the forward detectors. This means of production arises from the fully elastic channel whose total cross section can be written as

$$\sigma_{pp \rightarrow p(\gamma\gamma \rightarrow \Delta^{\pm\pm} \Delta^{\mp\mp})p} = \iint \sigma_{\gamma\gamma \rightarrow \Delta^{\pm\pm} \Delta^{\mp\mp}} \gamma_1^{el}(z_1) \gamma_2^{el}(z_2) dz_1 dz_2, \quad (10)$$

where $\gamma_{1/2}^{el}(z_{1/2})$ are γ -PDFs, distribution functions of the elastic equivalent photon in a proton with $z_{1/2}$ being momentum fractions. Elastic γ -PDFs indicate the probability

that a proton radiates a photon elastically while it remains undamaged itself, analytic expressions of which can be found in [55, 56]. The convolution integral over the momenta should not be taken over the whole range of parametric space, as the forward detectors measure final protons with various efficiencies depending on the proton energy loss $\xi \equiv 1 - E_{\text{out}}/E_{\text{in}}$, with $E_{\text{in/out}}$ referring to energies of the ingoing/outgoing protons. These effects are taken into account by translating the tagging efficiencies for protons to the ones for the elastic photons, which we discuss below.

To realize a better sensitivity in the hadronic environment at the LHC, we assume $v_\Delta < 10^{-4}$ GeV as discussed in the previous section and decay the doubly charged Higgs bosons into pairs of leptons (e^\pm or μ^\pm). Such a process through elastic photon fusion can then be expressed as

$$pp \rightarrow p(\gamma\gamma \rightarrow \Delta^{++} \Delta^{--} \rightarrow \ell_1^+ \ell_2^+ \ell_3^- \ell_4^-)p, \quad (11)$$

where $\ell_{1,2,3,4}$ can be different combinations of lepton flavors. Corresponding Feynman diagrams are displayed in Fig. 1, drawn using the TikZ-Feynman package [57]. According to the expression of decay width in Eq. (8), although the nature of neutrino mass is still unknown as it is sensitive to the neutrinoless double beta decay experiment, the oscillation data can, to a large extent, fix some elements of the neutrino mass matrix \mathcal{M}_ν and, subsequently, the branching ratios of certain leptonic decay channels. In our following simulation, we adopt the best-fit values for neutrino mixing parameters for the NH and IH cases [58, 59]

$$\begin{aligned} \text{NH: } \quad & \Delta m_{21}^2 = 7.49 \times 10^{-5} \text{eV}^2, \\ & \Delta m_{31}^2 = 2.513 \times 10^{-3} \text{eV}^2, \\ & \sin^2 \theta_{12} = 0.308, \quad \sin^2 \theta_{23} = 0.470, \\ & \sin^2 \theta_{13} = 0.02215, \quad \delta_{\text{CP}} = 212^\circ, \end{aligned} \quad (12)$$

$$\begin{aligned} \text{IH: } \quad & \Delta m_{21}^2 = 7.49 \times 10^{-5} \text{eV}^2, \\ & \Delta m_{31}^2 = -2.484 \times 10^{-3} \text{eV}^2, \\ & \sin^2 \theta_{12} = 0.308, \quad \sin^2 \theta_{23} = 0.550, \\ & \sin^2 \theta_{13} = 0.02231, \quad \delta_{\text{CP}} = 274^\circ. \end{aligned} \quad (13)$$

Note that two Majorana phases are assumed to vanish, and the lightest neutrino mass is adopted as 10^{-4} eV. With these best-fit values input, the leading decay channel is $\Delta^{\pm\pm} \rightarrow \mu^\pm \tau^\pm$ (BR \sim 35%) for the NH case and $\Delta^{\pm\pm} \rightarrow e^\pm e^\pm$ (BR \sim 47%) for the IH case [60]. Considering the better detection efficiencies at the LHC experiments for electrons and muons, we choose only electrons and

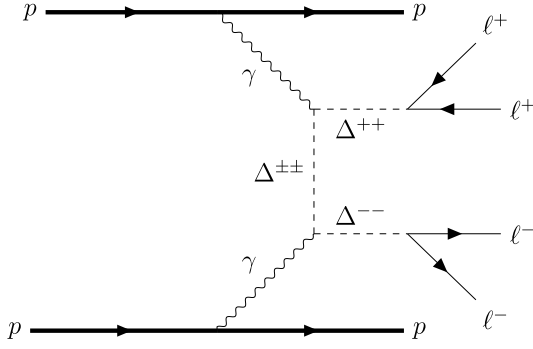


Fig. 1. Feynman diagram for the signal process of fully leptonic channel from doubly charged scalar pair production through elastic photon fusion at the LHC.

muons in the final states as our signals, where both scalars decay into $\ell_{1-4} = \mu$ (BR \sim 25% for $\Delta^{\pm\pm} \rightarrow \mu^{\pm}\mu^{\pm}$ under the above assumptions for neutrino mixing [60]) for NH and $\ell_{1-4} = e$ for IH. Figure 2 displays cross sections for these processes versus the triplet scalar mass ranging from 200 GeV to 2 TeV, where the difference of branching ratios of Δ decaying into different lepton flavors also manifests itself, as discussed above: for NH, the muon channel surpasses the electron one, and vice versa for IH.

The SM background corresponding to the above signals includes direct production of charged leptons through elastic photon fusion associated with a Z/γ decaying into a lepton pair (Fig. 3(a)), as well as a W pair production through the photon fusion associated with a Z/γ (Fig. 3(b)), with two intact protons in the final state:

$$pp \rightarrow p(\gamma\gamma \rightarrow \ell^+ \ell^- Z/\gamma \rightarrow \ell^+ \ell^- \ell^+ \ell^-)p, \quad (14)$$

$$pp \rightarrow p(\gamma\gamma \rightarrow W^+ W^- Z/\gamma \rightarrow \ell^+ \nu \ell^- \bar{\nu} \ell^+ \ell^-)p. \quad (15)$$

In the above diagrams, the mediating gauge boson Z/γ is shown going through the s -channel, while a t -channel contribution is also considered but not shown in the figures for simplicity. Similar to the process in Fig. 3(b), the associated production of two light jets along with the photon fusion into two W bosons can also mimic the signal when the jets are misidentified as leptons, so the following process is also considered as one of our backgrounds (Fig. 3(c)):

$$pp \rightarrow p(\gamma\gamma \rightarrow W^+ W^- jj \rightarrow \ell^+ \nu \ell^- \bar{\nu} jj)p. \quad (16)$$

Another background is top quark pair production through EPA photon fusion, followed by the top leptonic decay (Fig. 3(d))

$$pp \rightarrow p(\gamma\gamma \rightarrow t\bar{t} \rightarrow b\ell^+ \nu \bar{b}\ell^- \bar{\nu})p, \quad (17)$$

which also contaminates the signal if b -jets are misidenti-

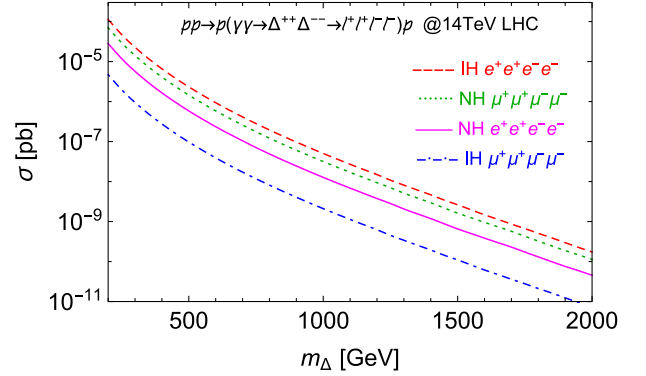


Fig. 2. (color online) Total cross sections of $pp \rightarrow p(\gamma\gamma \rightarrow \ell^+ \ell^+ \ell^- \ell^-)p$ with 4-electron and 4-muon final states for both NH and IH of neutrino mass spectra.

fied as leptons.

IV. SEARCH STRATEGIES AND RESULTS

To arrive at an effective search strategy for the fully leptonic channel from the doubly charged scalar at the LHC, we perform simulations using MADGRAPH5_AMC@NLO (v3.5.6) [61] for parton-level event generation and calculations for cross sections. Parton showering and detector simulation are realized by PYTHIA-8.2 [62] and DELPHES-3.5.0 [63] embedded in CHECKMATE2 [64] for further analysis and event selection. For model files, we use the TYPEIISEESAW UNIVERSAL FEYNRULES OUTPUT (UFO) libraries developed in [38]. γ -UPC packages [65] are used as γ -PDF for event generation of elastic photon fusion in the UPC of protons.

One of the most characteristic features of the signal is the final two intact protons, and, as discussed in Section III, they are not 100% detectable by the forward detectors at the LHC, but rather measured at some rates depending on their energy losses. In view of the elastic nature of the UPC, the energies of elastic photons E_γ emitted from the protons can be considered equal to the energy losses. For E_γ from 100 GeV to 1 TeV, the detection rate for final protons approximates 100% at the 13 TeV LHC, which can be translated to the energy loss ξ of (0.015, 0.15) defined in Section III [35, 36]. In our simulation, we adopt more conservative detection rates (Table 1) because lower efficiencies around 90% are generally indicated by phenomenological studies [40]. These values of proton tagging rates are then applied to the generated events, leaving only part of the events for further selection. This procedure can be viewed as a pre-selection in which the four-momenta of final protons are smeared with a 5%-width Gaussian function prior to the tagging rate application to realize the forward detector simulation. We use the PYLHE [66] package to process the MG5-generated events and for smearing.

Events surviving the pre-selection then go through

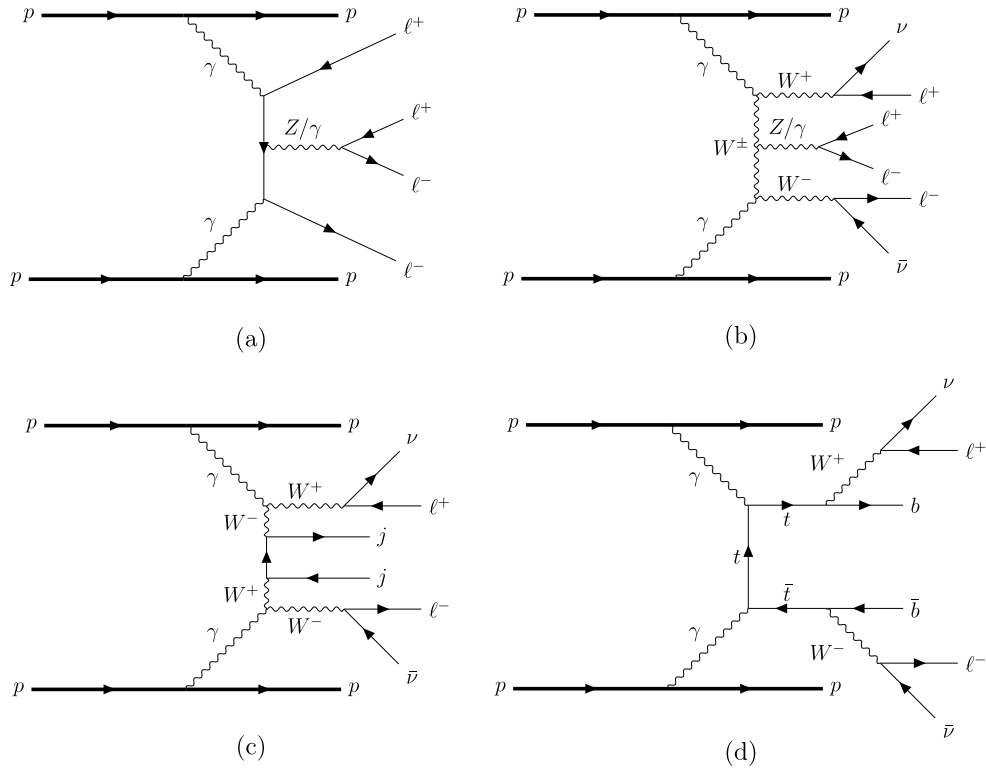


Fig. 3. Feynman diagrams of the Standard Model background for fully leptonic channels through elastic photon fusion at the LHC. t -channel Z/γ -mediating diagrams in (a) and (b) are not shown but taken into consideration in our analysis.

Table 1. Acceptance rates for initial photons for different ranges of energies, which are equivalent to tagging efficiencies for the outgoing protons corresponding to their energy losses [35, 36].

E_γ/GeV	(0,100]	(100,120]	(120,150]	(150,400]	(400, +∞)
Eff.	0	50%	70%	90%	80%

further cuts based on different features of kinematic distributions for the signal and background. For illustration, we present the histograms of three typical kinematic variables for signal and background events in Fig. 4, including the number of electrons (muons), transverse momentum of the leading electron (muon), and invariant mass of same-sign electrons (muons) for the inverted (normal) hierarchy. As examples, the benchmarks are chosen as $m_\Delta = 500$ and 1000 GeV, and the final states correspond to Eq. (11) with $\ell = e$ (for IH) and $\ell = \mu$ (for NH), while the histograms for background correspond to Eqs. (14) to (17). For simplicity, we show only one of the neutrino mass hierarchies in each figure of kinematic distributions. The histograms corresponding to the other hierarchy are not shown here, as they behave similarly to the displayed one. One can see from Figs. 4(a) and (b) that the number of electrons or muons for either IH or NH centers around 4, while for the SM backgrounds, the distributions peak around a much smaller electron or muon number. Because each pair of the final same-sign leptons in the signal events comes from the decay of a heavy

scalar, their momenta tend to be much larger than those in the background events. Moreover, as the mass of Δ increases, the peak values grow larger as well, which can be seen clearly from the distributions of leading lepton p_T in Figs. 4(c) and (d). Hence, one of the key features to distinguish the signal from backgrounds is multiple leptons with high p_T . Another distinctive feature of the signal also comes from Δ decay, as displayed in Fig. 4(e) and (f), showing distributions of the invariant mass reconstructed from same-sign electrons or muons. For signal events, the histograms exhibit clear endpoints centering around the values of m_Δ , while the background ones peak at a smaller range with relatively longer tails.

Based on the above kinematic distributions for $4e$ events in the IH case and 4μ events in the NH case, we perform event selections (Table 2) to achieve a better signal significance for each case. As discussed, as the final two intact protons are detected with certain efficiencies (Table 1), we can regard this procedure as a step of pre-selection of the events. Then, two pairs of opposite same-sign electrons ($e^+e^+e^-e^-$) and muons ($\mu^+\mu^+\mu^-\mu^-$) are re-

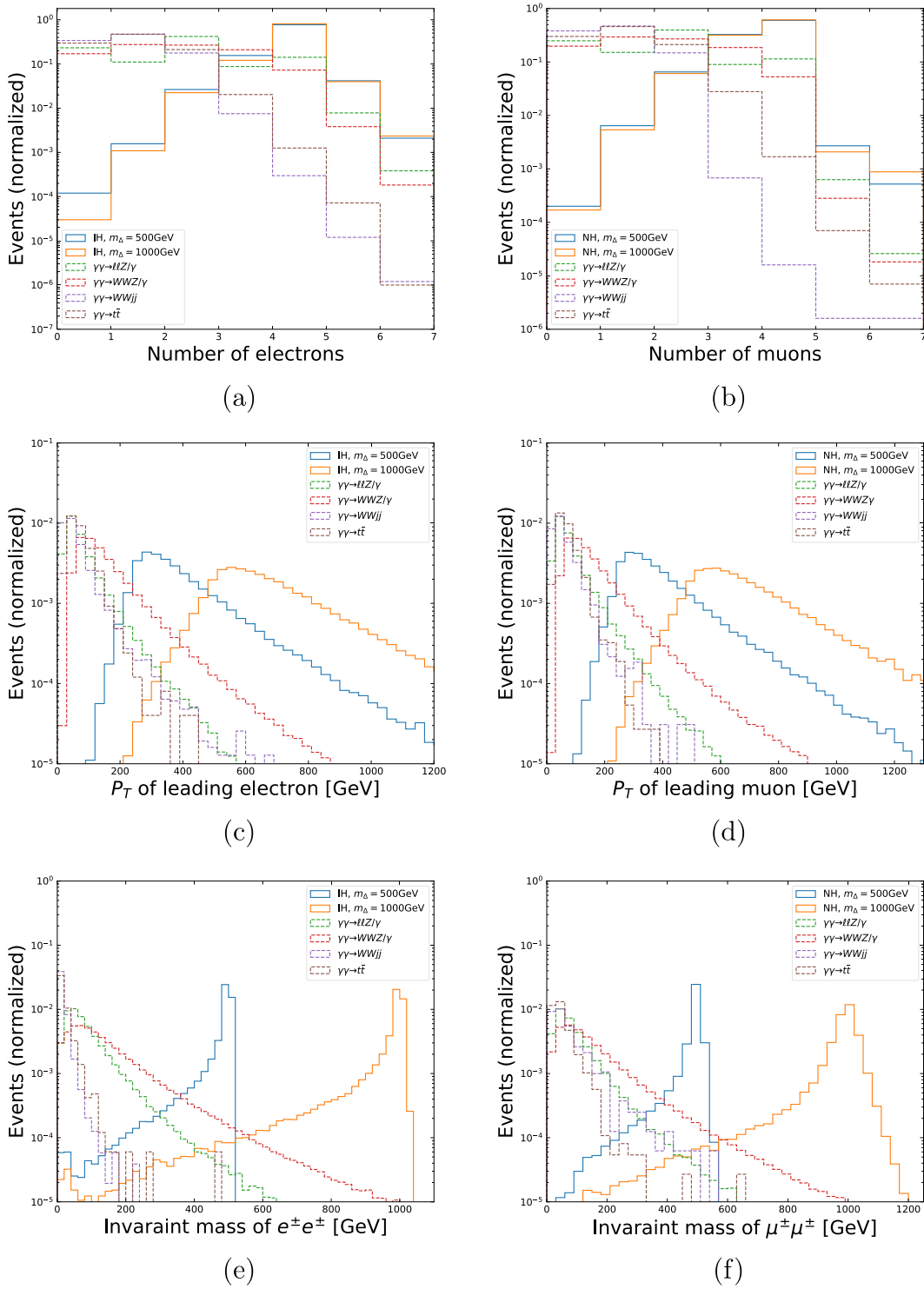


Fig. 4. (color online) Kinematic distributions of electron (muon) number, transverse momentum of the leading electron (muon), and invariant mass of same-sign electrons (muons) from elastic photon fusion at the LHC: $pp \rightarrow p(\gamma\gamma \rightarrow \Delta^{++}\Delta^{--} \rightarrow \ell^+\ell^+\ell^-\ell^-)p$ for inverted (normal) hierarchy spectrum as signal, as well as for four SM background processes at the LHC. Histograms for the signals are shown as solid lines, and those for backgrounds are shown as dashed lines.

quired as cut-1 for IH and NH, respectively. Cut-2 is $p_T > 50$ GeV for the leading lepton and cut-3 on the invariant mass of the pair of same-sign leptons $m(\ell^+\ell^+)$. To realize a relatively optimal selection strategy and signal

significance, we apply specific selection criteria on $m(\ell^+\ell^+)$ to each benchmark point of m_Δ . For the final states of $e^+e^+e^-e^-$ in the signal region of IH, cut-3 is adopted as $m(e^+e^+) \in [m_\Delta - 25, m_\Delta + 15]$ GeV, while for

Table 2. Event selections for signal processes with final states of $e^+e^+e^-e^-$ and $\mu^+\mu^+\mu^-\mu^-$, corresponding to IH and NH, respectively. Units of p_T and masses are GeV, which are omitted in the table for simplicity.

Cuts	Signal	
	$e^+e^+e^-e^-$, IH	$\mu^+\mu^+\mu^-\mu^-$, NH
Pre-selection	Two outgoing protons tagged	
Cut-1	$e^+e^+e^-e^-$	$\mu^+\mu^+\mu^-\mu^-$
Cut-2	Leading e/μ $p_{T>50}$	
Cut-3	$m(e^\pm e^\pm) \in [m_\Delta - 25, m_\Delta + 15]$	$m(\mu^\pm \mu^\pm) \in [m_\Delta - 20, m_\Delta + 20]$

$\mu^+\mu^+\mu^-\mu^-$ final states in the signal region of NH, cut-3 is $m(\mu^\pm \mu^\pm) \in [m_\Delta - 20, m_\Delta + 20]$ GeV. As examples, Tables 3 and 4 display cutflows of effective cross sections for the signal and background through these cuts for $m_\Delta = 500$ and 850 GeV under NH and IH, respectively. For both cases, we can see from the tables that cut-1 on leptonic multiplicities can largely suppress the backgrounds of W^+W^-jj and $t\bar{t}$ events, while cut-3 on invariant mass of same-sign lepton pairs can basically filter out the other two: $\ell^+\ell^-Z/\gamma$ and W^+W^-Z/γ .

Masses of the doubly charged scalar are scanned in increments of 50 GeV from 200 to 1500 GeV under both IH and NH spectra of neutrino mass. Event selections are then applied according to Table 2 with regard to two different final states of $e^+e^+e^-e^-$ and $\mu^+\mu^+\mu^-\mu^-$ under neutrino mass spectra of IH and NH, respectively. The expected significance is finally calculated for each scanned point of m_Δ using the formula

$$\alpha = S/\sqrt{B+(\beta B)^2}, \quad (18)$$

where $S(B)$ refers to signal (background) events after the event selections in Table 2 and β the systematic uncertainty. Given the parameters input for the neutrino mixing matrix in the cases of IH and NH (Eq. (13) and (12)), we obtain the luminosities needed to arrive at 2σ exclusion limits for every scanned m_Δ , whose fitted curves are shown in Fig. 5. For luminosities of 36.1 fb^{-1} , 100 fb^{-1} and 3 ab^{-1} , 2σ exclusion limits are also obtained for the branching ratios of $\Delta \rightarrow \mu\mu$ for NH and those of $\Delta \rightarrow ee$ for IH at each point of m_Δ . Figure 6 shows contours in the parametric space of the diagonal branching ratios versus m_Δ . As a comparison, exclusion bounds are also presented from searching for prompt same-sign lepton pairs by the ATLAS experiment [67–69] at 7, 8, and 13 TeV with 4.7, 20.3, and 36.1 fb^{-1} integrated luminosities, respectively.

From Figs. 5 and 6, one can infer that sensitivities for $e^+e^+e^-e^-$ final states are better than those for $\mu^+\mu^+\mu^-\mu^-$. This performance results partly from our assumptions for NH and IH neutrino mass spectra, under which the Δ decay branching ratio into electrons ($\sim 47\%$) is larger than that into muons ($\sim 25\%$). As m_Δ increases, the cross sections of elastic photon fusion production of $\Delta^{++}\Delta^{--}$ decrease rapidly, leading to lower sensitivities for branching ratios in the range of larger masses, as expected (see solid lines in Fig. 2). Similar behavior of exclusion curves can be seen in the searches through Drell-Yan production followed by multileptonic final states (see dashed lines in

Table 3. Effective cross sections of the signal process $pp \rightarrow p(\gamma\gamma \rightarrow \Delta^{++}\Delta^{--} \rightarrow \mu^+\mu^+\mu^-\mu^-)p$ after each step of cutflow under NH neutrino mass spectrum with $m_{\Delta^\pm} = 500$ GeV, and of four SM backgrounds, $\ell^+\ell^-Z/\gamma$, W^+W^-Z/γ , W^+W^-jj and $t\bar{t}$ events, from elastic photon fusion at the 14 TeV LHC. Cross sections and masses are in units of picobarn and GeV, respectively, which are omitted in the table for simplicity.

	$m_\Delta = 500$ NH	$\ell^+\ell^-Z/\gamma$	W^+W^-Z/γ	W^+W^-jj	$t\bar{t}$
No cuts	1.45×10^{-6}	8.52×10^{-6}	4.68×10^{-7}	2.55×10^{-3}	7.71×10^{-6}
2 protons	9.63×10^{-7}	9.01×10^{-7}	2.45×10^{-7}	4.88×10^{-4}	3.15×10^{-6}
$2\mu^+2\mu^-$	5.86×10^{-7}	1.24×10^{-7}	1.37×10^{-8}	5.10×10^{-9}	4.04×10^{-9}
High p_T	5.86×10^{-7}	1.10×10^{-7}	1.34×10^{-8}	2.55×10^{-9}	2.82×10^{-9}
$m(\mu^\pm \mu^\pm)$	4.69×10^{-7}	9.46×10^{-10}	1.08×10^{-10}	0	0

Table 4. Same as Table 3 but for the signal process $pp \rightarrow p(\gamma\gamma \rightarrow \Delta^{++}\Delta^{--} \rightarrow e^+e^+e^-e^-)p$ under IH neutrino mass spectrum with $m_{\Delta^\pm} = 850$ GeV.

	$m_\Delta = 850$ IH	$\ell^\pm \ell^\pm Z/\gamma$	WWZ/γ	$WWjj$	$t\bar{t}$
No cuts	1.37×10^{-7}	8.52×10^{-6}	4.68×10^{-7}	2.55×10^{-3}	7.71×10^{-6}
2 protons	8.87×10^{-8}	9.01×10^{-7}	2.45×10^{-7}	4.88×10^{-4}	3.15×10^{-6}
$2e^+2e^-$	7.47×10^{-8}	1.54×10^{-7}	1.87×10^{-8}	1.28×10^{-7}	3.04×10^{-9}
High p_T	7.47×10^{-8}	1.37×10^{-7}	1.83×10^{-8}	9.95×10^{-8}	2.22×10^{-9}
$m(e^\pm e^\pm)$	5.54×10^{-8}	4.26×10^{-11}	1.65×10^{-11}	0	0

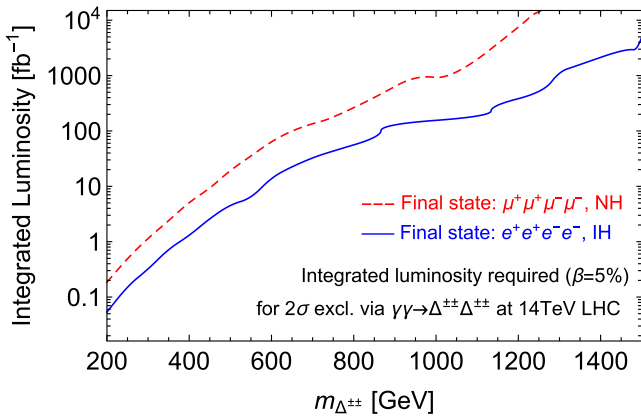


Fig. 5. (color online) Integrated luminosities required to reach 2σ exclusion searching for fully elastic photon fusion $pp \rightarrow p(\gamma\gamma \rightarrow \Delta^{++}\Delta^{--} \rightarrow \ell^+\ell^+\ell^-\ell^-)p$ at the 14 TeV LHC. Systematic uncertainty β is assumed as 5%. Red dashed lines correspond to $\mu^+\mu^+\mu^-\mu^-$ state in case of NH, while blue solid lines correspond to $e^+e^+e^-e^-$ state in case of IH.

Fig. 2 [69]). However, comparing these results, it can be seen that for both $e^+e^+e^-e^-$ and $\mu^+\mu^+\mu^-\mu^-$ states, the sensitivity for branching ratios via elastic photon fusion decreases more slowly and smoothly as m_Δ grows than that of the Drell-Yan production searches. For example, in the mass range below 650 GeV, the Drell-Yan production search can probe smaller branching ratios $\text{Br}(\Delta^{\pm\pm} \rightarrow e^+e^+) < 40\%$ at $\mathcal{L} = 36.1 \text{ fb}^{-1}$. For a relatively larger mass range beyond 650 GeV, the photon fusion search of the present work displays better sensitivity and can extend the 2σ exclusion limit to the TeV region for similar branching ratios (see black solid lines in Fig. 6). For the probing sensitivity for branching ratio $\text{Br}(\Delta^{\pm\pm} \rightarrow \mu^+\mu^+)$, photon fusion search exceeds the Drell-Yan search in the mass range larger than 750 GeV with $\mathcal{L} = 36.1 \text{ fb}^{-1}$. Similar advantages of the photon fusion search across larger

mass range can also be seen in other luminosity scenarios (see blue and red solid lines in Fig. 6 for $\mathcal{L} = 100 \text{ fb}^{-1}$ and 3 ab^{-1}).

Specifically, with a collision energy of 14 TeV and integrated luminosity of 36.1 fb^{-1} , a 2σ exclusion limit for m_Δ can reach 730 GeV for $\text{Br}(\Delta \rightarrow ee) \sim 47\%$ under the IH spectrum and surpasses the limits given by the ATLAS experiment at $m_\Delta \sim 685 \text{ GeV}$ [69]. With higher luminosities of 100 fb^{-1} and 3 ab^{-1} , this bound can be extended to $m_\Delta \sim 880 \text{ GeV}$ and 1.5 TeV , respectively. However, considering the angular limitation of forward detectors for outgoing protons, there exists an upper limit for forward detectors on the invariant mass of final states around 2.6 TeV [45]. For the case of pair production of the doubly charged scalars $\Delta^{\pm\pm}$, each one has an upper mass limit around 1.3 TeV that the forward detectors can reach. Hence, the exclusion limit of 1.5 TeV obtained in the case of IH spectrum with $\mathcal{L} = 3 \text{ ab}^{-1}$, exceeding the 1.3 TeV upper bound set by the detector itself, should be lowered to 1.3 TeV. Meanwhile, with luminosities of 36.1 fb^{-1} and 100 fb^{-1} the results through $\mu^+\mu^+\mu^-\mu^-$ search are less promising, excluding at 95% C.L. around $m_\Delta \sim 430$ and 520 GeV , respectively, for $\text{Br}(\Delta \rightarrow \mu\mu) \sim 25\%$ under the NH spectrum. However, with a higher luminosity of 3 ab^{-1} , the mass exclusion bound can be improved up to $m_\Delta \sim 1 \text{ TeV}$, surpassing the limit set by the ATLAS experiment at $m_\Delta \sim 620 \text{ GeV}$ [69].

It should be noted that the enhancement in the sensitivity to $e^+e^+e^-e^-$ final states in the IH case compared to that of $\mu^+\mu^+\mu^-\mu^-$ states in the NH case largely relies on the enhanced branching ratio of the exotic scalar decaying into electrons. This enhancement is sensitive to the assumed lightest neutrino mass of 10^{-4} eV , the increase of which will reduce the distinction between branching ratios into leptons of different flavors. Hence, the conclusions for mass exclusion hold for our chosen parameters,

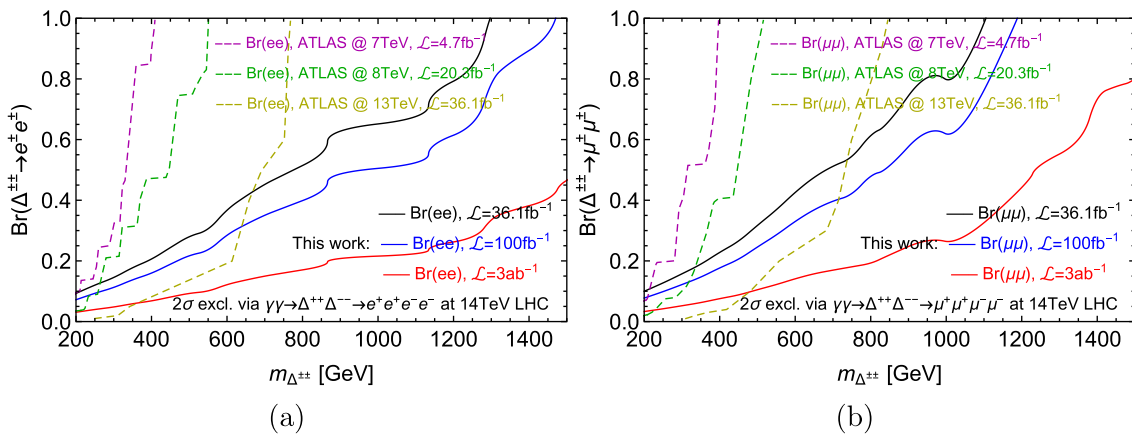


Fig. 6. (color online) Branching ratios that can be excluded at 95% C.L. via searching for fully elastic photon fusion $pp \rightarrow p(\gamma\gamma \rightarrow \Delta^{++}\Delta^{--} \rightarrow \ell^+\ell^+\ell^-\ell^-)p$ at the 14 TeV LHC, shown as black ($\mathcal{L} = 36.1 \text{ fb}^{-1}$), blue ($\mathcal{L} = 100 \text{ fb}^{-1}$) and red ($\mathcal{L} = 3 \text{ ab}^{-1}$) solid lines. Systematic uncertainty β is assumed as 5%. (a) and (b) are for branching ratios of $\Delta^{\pm\pm} \rightarrow e^\pm e^\pm$ and $\mu^\pm \mu^\pm$, respectively. Dashed lines are bounds from the ATLAS experiment [67–69].

especially in the neutrino sector. Note also that the contours shown in Fig. 6 from the ATLAS experiment and the present work both assume a tiny $\nu_\Delta < 10^{-4}$ GeV, so only dileptonic decay modes are relevant. Meanwhile, under the assumption of $\nu_\Delta > 10^{-4}$ GeV and dominant dibosonic decay, the decay channels $\Delta^{\pm\pm} \rightarrow W^\pm W^\pm$ have also been thoroughly searched for at the 13 TeV LHC, as discussed in Section II. However, due to a larger hadronic background at the hadron collider, weaker bounds on m_Δ were obtained around 200–350 GeV for degenerate or non-degenerate mass spectra using $36.1\sim 139$ fb $^{-1}$ collected events [31, 33].

V. CONCLUSION

We study the sensitivities for pair production of doubly charged scalars within the type-II seesaw mechanism (with a degenerate mass spectrum of the scalar components) through elastic photon fusion at the 14 TeV LHC: $pp \rightarrow p(\gamma\gamma \rightarrow \Delta^{++}\Delta^{--})p$. Two types of neutrino

mass spectra, NH and IH, are considered. In the case of NH, final states of $\mu^+\mu^+\mu^-\mu^-$ are studied as the signal process with integrated luminosities of 36.1 fb $^{-1}$, 100 fb $^{-1}$, and 3 ab $^{-1}$, the 2σ exclusion limits on m_Δ can reach approximately 430, 520, and 1000 GeV respectively, for branching ratio of $\Delta^{\pm\pm} \rightarrow \mu^\pm\mu^\pm \sim 25\%$, which is set by adopting the best-fit values of the PMNS matrix under the NH spectrum. In the case of IH and a largely fixed branching ratio $\Delta^{\pm\pm} \rightarrow e^\pm e^\pm \sim 47\%$, final states of $e^+e^+e^-e^-$ are studied as signal under the same luminosities with the exclusion bounds on m_Δ reaching approximately 730, 880, and 1300 GeV, corresponding to the above luminosities.

ACKNOWLEDGMENTS

We are grateful to David d'Enterría and Hua-Sheng Shao for their helpful discussions on γ -PDFs. We also express many thanks to Marek Tasevsky for useful discussions.

References

- [1] S. Weinberg, *Phys. Rev. Lett.* **43**, 1566 (1979)
- [2] P. Minkowski, *Phys. Lett. B* **67**, 421 (1977)
- [3] T. Yanagida, *Proceedings of the Workshop on Unified Theory and the Baryon Number of the Universe*, ed. O. Sawada and A. Sugamoto (Tsukuba 1979)
- [4] R. N. Mohapatra and G. Senjanović, *Phys. Rev. Lett.* **44**, 912 (1980)
- [5] J. Schechter and J. W. F. Valle, *Phys. Rev. D* **22**, 2227 (1980)
- [6] T. P. Cheng and L. F. Li, *Phys. Rev. D* **22**, 2860 (1980)
- [7] M. Magg and C. Wetterich, *Phys. Lett. B* **94**, 61 (1980)
- [8] R. N. Mohapatra and G. Senjanović, *Phys. Rev. D* **23**, 165 (1981)
- [9] G. Lazarides, Q. Shafi, and C. Wetterich, *Nucl. Phys. B* **181**, 287 (1981)
- [10] R. Foot, H. Lew, X.G. He *et al.*, *Z. Phys. C* **44**, 441 (1989)
- [11] E. Ma, *Phys. Rev. Lett.* **81**, 1171 (1998)
- [12] G. Senjanovic, *Nucl. Phys. B* **153**, 334 (1979)
- [13] G. 't Hooft, *NATO Sci. Ser. B* **59**, 135 (1980)
- [14] D. K. Ghosh, N. Ghosh, I. Saha *et al.*, *Phys. Rev. D* **97**(11), 115022 (2018)
- [15] A. Crivellin, M. Ghezzi, L. Panizziet *et al.*, *Phys. Rev. D* **99**(3), 035004 (2019)
- [16] P. S. Bhupal Dev and Y. Zhang, *JHEP* **10**, 199 (2018)
- [17] M. M. Altakach, P. Lamba, R. Masešek *et al.*, *Eur. Phys. J. C* **82**(9), 848 (2022)
- [18] A. Das, S. Mandal, and S. Shil, *Phys. Rev. D* **108**(1), 015022 (2023)
- [19] A. Das, J. Li, S. Mandal *et al.*, *Phys. Rev. D* **112**(3), 035008 (2025)
- [20] M. A. Arroyo-Ureña, O. Félix-Beltrán, J. Hernández-Sánchez *et al.*, *Phys. Rev. D* **112**(1), 015021 (2025)
- [21] J. C. Pati and A. Salam, *Phys. Rev. D* **10**, 275 (1974) [Erratum: *Phys. Rev. D* **11**, 703 (1975)]
- [22] R. N. Mohapatra and J. C. Pati, *Phys. Rev. D* **11**, 566 (1975)
- [23] G. Senjanovic and R. N. Mohapatra, *Phys. Rev. D* **12**, 1502 (1975)
- [24] A. Zee, *Nucl. Phys. B* **264**, 99 (1986)
- [25] K. S. Babu, *Phys. Lett. B* **203**, 132 (1988)
- [26] M. S. Chanowitz and M. Golden, *Phys. Lett. B* **165**, 105 (1985)
- [27] H. Georgi and M. Machacek, *Nucl. Phys. B* **262**, 463 (1985)
- [28] Y. Cai, T. Han, T. Li *et al.*, *Front. in Phys.* **6**, 40 (2018)
- [29] M. Muhlleitner and M. Spira, *Phys. Rev. D* **68**, 117701 (2003)
- [30] G. Aad *et al.* (ATLAS Collaboration), *Eur. Phys. J. C* **83**(7), 605 (2023)
- [31] M. Aaboud *et al.* (ATLAS Collaboration), *Eur. Phys. J. C* **79**(1), 58 (2019)
- [32] A. Melfo, M. Nemevsek, F. Nesti *et al.*, *Phys. Rev. D* **85**, 055018 (2012)
- [33] G. Aad *et al.* (ATLAS Collaboration), *JHEP* **06**, 146 (2021)
- [34] E. J. Chun, H. M. Lee and P. Sharma, *JHEP* **11**, 106 (2012)
- [35] M. Albrow *et al.* (CMS and TOTEM Collaborations), CERN-LHCC-2014-021
- [36] L. Adamczyk, E. Banaś, A. Brandt *et al.*, CERN-LHCC-2015-009
- [37] T. Han, B. Mukhopadhyaya, Z. Si *et al.*, *Phys. Rev. D* **76**, 075013 (2007)
- [38] B. Fuks, M. Nemevšek, and R. Ruiz, *Phys. Rev. D* **101**(7), 075022 (2020)
- [39] L. A. Harland-Lang, V. A. Khoze, M. G. Ryskin *et al.*, *JHEP* **04**, 010 (2019)
- [40] L. Beresford and J. Liu, *Phys. Rev. Lett.* **123**(14), 141801 (2019)
- [41] S. I. Godunov, V. A. Novikov, A. N. Rozanov *et al.*, *JHEP* **01**, 143 (2020)
- [42] H. Zhou and N. Liu, *JHEP* **10**, 092 (2022)
- [43] H. Zhou and N. Liu, *Nucl. Phys. B* **1010**, 116752 (2025)
- [44] K. S. Babu and S. Jana, *Phys. Rev. D* **95**(5), 055020 (2017)
- [45] L. Duarte, V. P. Goncalves, D. E. Martins *et al.*, *Phys. Rev. D* **107**(3), 035010 (2023)

- [46] L. Duarte, V. P. Goncalves, D. E. Martins *et al.*, *Eur. Phys. J. C* **84**(7), 709 (2024) [Erratum: *Eur. Phys. J. C* **84**(12), 1328 (2024)]
- [47] P. Fileviez Perez, T. Han, G. y. Huang *et al.*, *Phys. Rev. D* **78**, 015018 (2008)
- [48] S. Mandal, O. G. Miranda, G. Sanchez Garcia *et al.*, *Phys. Rev. D* **105**(9), 095020 (2022)
- [49] S. Navas *et al.* (Particle Data Group), *Phys. Rev. D* **110**(3), 030001 (2024)
- [50] U. Bellgardt *et al.* (SINDRUM Collaboration), *Nucl. Phys. B* **299**, 1 (1988)
- [51] A. M. Baldini *et al.* (MEG Collaboration), *Eur. Phys. J. C* **76**(8), 434 (2016)
- [52] D. N. Dinh, A. Ibarra, E. Molinaro *et al.*, *JHEP* **08**, 125 (2012) [Erratum: *JHEP* **09**, 023 (2013)]
- [53] S. Ashanujjaman and K. Ghosh, *JHEP* **03**, 195 (2022)
- [54] E. J. Chun, K. Y. Lee, and S. C. Park, *Phys. Lett. B* **566**, 142 (2003)
- [55] V. M. Budnev, I. F. Ginzburg, G. V. Meledin *et al.*, *Phys. Rept.* **15**, 181 (1975)
- [56] B. A. Kniehl, *Phys. Lett. B* **254**, 267 (1991)
- [57] J. Ellis, *Comput. Phys. Commun.* **210**, 103 (2017)
- [58] I. Esteban, M. C. Gonzalez-Garcia, M. Maltoni *et al.*, *JHEP* **12**, 216 (2024)
- [59] NuFIT 6.0 (2024), www.nu-fit.org
- [60] T. Li, C. Y. Yao, and M. Yuan, *JHEP* **03**, 137 (2023)
- [61] J. Alwall, R. Frederix, S. Frixione *et al.*, *JHEP* **07**, 079 (2014)
- [62] T. Sjöstrand, S. Ask, J. R. Christiansen *et al.*, *Comput. Phys. Commun.* **191**, 159 (2015)
- [63] J. de Favereau *et al.* (DELPHES 3 Collaboration), *JHEP* **02**, 057 (2014)
- [64] D. Dercks, N. Desai, J. S. Kim *et al.*, *Comput. Phys. Commun.* **221**, 383 (2017)
- [65] H. S. Shao and D. d'Enterria, *JHEP* **09**, 248 (2022)
- [66] L. Heinrich, M. Feickert, and E. Rodrigues, pylhe: v0.3.0 <https://github.com/scikit-hep/pylhe/tree/v0.3.0>
- [67] G. Aad *et al.* (ATLAS Collaboration), *Eur. Phys. J. C* **72**, 2244 (2012)
- [68] G. Aad *et al.* (ATLAS Collaboration), *JHEP* **03**, 041 (2015)
- [69] M. Aaboud *et al.* (ATLAS Collaboration), *Eur. Phys. J. C* **78**(3), 199 (2018)